Simplified Mathematical Modeling of Implant Limit Stress and Maximum HAZ Hardness

Models were developed to form a simple, accessible tool for use in assessing susceptibility to hydrogen-induced cracking in steel weldments

BY A. FOTOUH, M. EL-SHENNAWY, AND R. EL-HEBEARY

ABSTRACT

Hydrogen-induced cracking (HIC) susceptibility in the heat-affected zone (HAZ) was investigated and modeled using implant static tensile limit stress (σ_{imp}) and maximum hardness of the HAZ (HV_{10MAX}). C-Mn and high-strength low-alloy (HSLA) steels were used as base metals with a carbon equivalent (CE) ranging from 0.38 to 0.48% and 0.52 to 0.69%, respectively. The shielded metal arc welding (SMAW) and gas metal arc welding (GMAW) processes with CO_2 shielding gas were used. The diffusible hydrogen (H) content was varied taking the values between 2 and 40 mL/100 g. σ_{imp} and HV_{10MAX} were the two measures used to evaluate the weldment susceptibility to HIC. Using Pearson's product-moment coefficient (P_{pm}) and the developed analysis of HIC susceptibility, two simplified models were developed using simple mechanistic models, linear and logarithmic, to simulate σ_{imp} and HV_{10MAX}. σ_{imp} was modeled as a function of HV_{10MAX} and H, while HV_{10MAX} was modeled as a function of CE and $t_{800/500}$. The two new simplified models were capable of accurately simulating both σ_{imp} and HV_{10MAX}. The newly developed models form a simplified tool that can be used to assess HIC susceptibility in steel weldments.

Introduction

Three main factors affect hydrogen-induced cracking (HIC) susceptibility in weldments. They are as follows (Refs. 1–3):

- Presence of hydrogen
- Residual stresses
- Susceptible microstructure.

The diffusible hydrogen (H) content is generally considered the effective fraction of hydrogen in weldments HIC (Refs. 2, 4–8). At relatively low temperature (i.e., between 100° and 200°C), the diffusible atomic hydrogen accumulated forms the molecule hydrogen, which has very high pressure at room temperature (Refs. 6, 9, 10). Therefore, HIC, which is sometimes known as cold cracking or delayed cracking (Refs. 6, 9), is formed after solidification of fusion welding. On the other hand, residual stresses developed during cooling take place at a comparatively low temperature, which increases the risk of HIC (Ref. 4), as HIC initiates when the stress and the strain induced at a point reaching critical values (Ref. 11). Hydrogen-induced cracking in the HAZ can be overcome, if the implant static tensile limit stress (σ_{imp}) determined at certain welding parameters or factors (i.e., H, carbon equivalent (CE), and $t_{800/500}$) exceeds the value of the residual stresses arising in the welded structure (Ref. 11).

Another factor affecting the presence of HIC is the susceptible microstructure (Refs. 1–3). In the case of HIC in the HAZ, typically it is sufficient to know the maximum HAZ hardness (HV_{10MAX}) to assess the HIC susceptibility of the developed HAZ microstructure, which is determined by (Refs. 4, 12–16): 1) the steel chemical composition (mainly CE and carbon content), and 2) the weld cooling time between 800° and 500°C ($t_{800/500}$) at which the austenitic transformations take place. Hydrogen-induced cracking susceptibility is increased by increasing HAZ hardness (Refs. 1–4, 9, 12–16).

Therefore, this present study was concerned with analyzing and modeling σ_{imp} and HV_{10MAX}, as they both form the main factors that can be used to assess susceptibility to HIC in steel weldments (Refs. 1–4, 11–16). Simplified models were developed to estimate the values of σ_{imp} and HV_{10MAX} as functions of welding factors (i.e., CE, $t_{800/500}$, and H).

KEYWORDS

Modeling
Hydrogen-Induced Cracking (HIC)
Implant Test
Implant Static Tensile Limit Stress
Maximum Heat-Affected Zone (HAZ) Hardness
Shielded Metal Arc Welding (SMAW)
Gas Metal Arc Welding (GMAW)

Testing Materials and Procedures

The designations of the tested steels and their mechanical properties are shown in Table 1. The Dearden and O'Neill equation, represented in Equation 1, was applied to calculate the CE for each one of the tested steels (Refs. 17–19). This equation is used for steels with carbon contents greater than 0.12%, and if the calculated CE is greater than 0.35%, special precautions should be considered to prevent HIC (Ref. 17). The Dearden and O'Neill equation is the formula used by the International Institute of Welding (IIW) to evaluate carbon equivalent (Ref. 20).

$$CE = C + (Mn)/6 + (Cr + Mo + V)/5 + (Cu + Ni)/15 \quad (1)$$

The calculated CE values are shown in Table 2. The tested base metals are divided into two main categories of steels:

1. C-Mn steels, which have CE values in the range of 0.38 to 0.48% and yield strength values in the range of 350 to 623 MPa.
2. High-strength, low-alloy (HSLA) steels, which have CE values in the range of 0.52 to 0.69% and yield strength range

A. FOTOUH (fotouh@ualberta.ca) *is a research assistant, Mechanical Engineering Dept., University of Alberta, Edmonton, Alberta, Canada. M. El-SHENNAWY is an associate professor, Mechanical Engineering Dept., Faculty of Engineering, Taif University, Taif, Saudi Arabia, and on leave from Helwan University, Faculty of Engineering, Mechanical Engineering Department. R. EL-HEBEARY is professor emeritus, Mechanical Design and Production Dept., Faculty of Engineering, Cairo University, Giza, Egypt.*

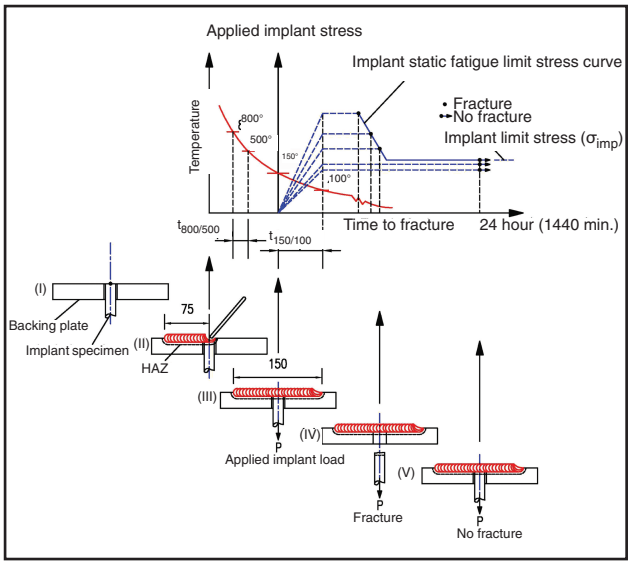

Fig. 1 — Schematic representing the applied implant test procedures.

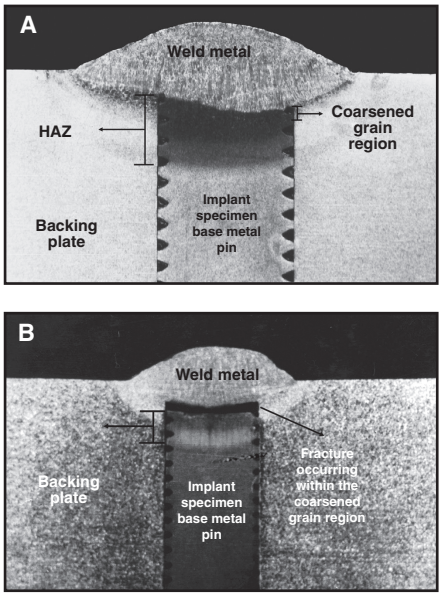

Fig. 2 — Sections of implant test specimen pins: A — Nonfractured; B — fractured.

between 295 and 710 MPa.

Different welding electrodes were used in this research using two welding processes: shielded metal arc welding (SMAW) and gas metal arc welding (GMAW) with CO_2 as a shielding gas. Table 3 shows the designation of the electrodes used along with their chemical composition and the mechanical properties of the deposited weld metal.

Using the glycerin displacement method, the diffusible hydrogen content was measured for each electrode type (Ref. 19). The procedures followed in the glycerin method were according to the designations of JIS Z 3113, JIS Z 3116, JIS Z 3117, and DIN 8572 Part I (Ref. 19). Table 4 shows the values of the measured diffusible hydrogen content for each type of deposited weld metal. The electrodes were used under the conditions in Table 4, which were the conditions the manufacturer recommended.

For each implant test, a 6.0±0.02-mm implant specimen was fitted into a 6.0–0.02-mm-diameter hole in a backing steel plate (Ref. 19). The backing plate was manufactured in two thicknesses of 10 and 30 mm simulating 2-D and 3-D weldments. The backing plate steel designation and mechanical properties are listed in Table 1, while its chemical composition is listed in Table 2.

Figure 1 shows the applied implant test procedures with a 150-mm weld bead on the backing plate. The applied implant test procedures are as follows:

1. The implant test is inserted into the backing plate hole.

2. When the electrode reaches the tip of the implant test specimen, cooling time is started to be counted.

3. The implant load is started to be applied when the temperature is 150°C, while the full applied implant load is reached when the temperature is 100°C.

4. The implant specimen is fractured within 24 h depending on the amount of the applied implant load.

5. If the implant specimen is not fractured after 24 h under a certain implant load, the corresponding stress to this load will be the implant static tensile limit stress (σ_{imp}). To ensure that the stress value reached was the value of σ_{imp}, five more specimens were tested at this stress value. The stress is considered to be σ_{imp}, if the five tested specimens are not fractured after 24 h.

The cooling time from 800° to 500°C ($t_{800/500}$) was measured using a thermocouple that was implanted into the backing plate in the same way the implant test specimen pins were implanted. The measured values of $t_{800/500}$ are shown in Table 5. In order to incorporate $t_{800/500}$ into the developed mathematical models and to consistently control the loading time of implant tests, a heat transfer thermal model was used to simulate the measured values of $t_{800/500}$ based on the applied welding conditions. Additionally, the use of the heat transfer model ensures that the developed mathematical models are a fully mathematical engineering tool that can be used directly to estimate the values of σ_{imp} and the values of HV_{10MAX} without the need to take any further measures.

Rosenthal's heat transfer models are usually used to estimate the weldment's cooling cycle (Refs. 3, 21, 22). For a radial distance near the weld, Adam's heat transfer models can be developed from Rosenthal's models (Ref. 19); therefore, Adam's models can be used to estimate the cooling time of the HAZ coarsened grain region near the weld (Refs. 9, 19, 21, 23). In this study, the Adam's heat transfer models

Table 1 — Mechanical Properties for Base Metals

Steel Type	Base Metal Sample	Steel Designation	Yield Strength, MPa	Mechanical Properties Ultimate Tensile Strength, MPa	Elongation, %
C-Mn	A	DIN: 17Mn4	350	580	37
	B	DIN: St 52-3N	420	595	30
	C	MSZ: E420C	623	775	21
HSLA	D	MSZ:KL3	295	535	23
	E	ASTM:387-G11	310	585	19
	F	DIN:20CrMo5	710	1150	7
Implant backing plate (heat sink)		DIN: St 37-2	260	320	54

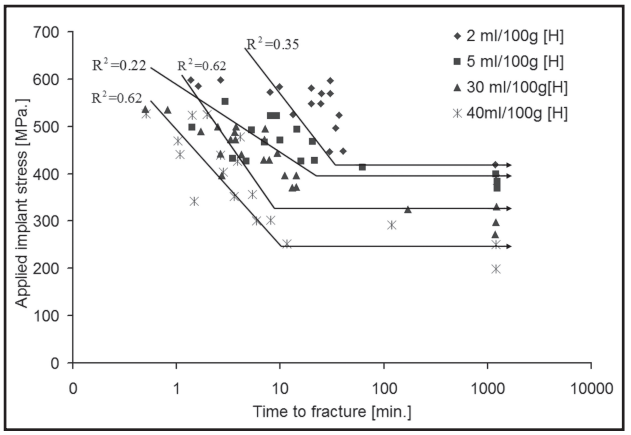

Fig. 3 — Effect of H on the implant test results for steel B: 0.42 (CE) and at $t_{800/500}$ of 4.5 s.

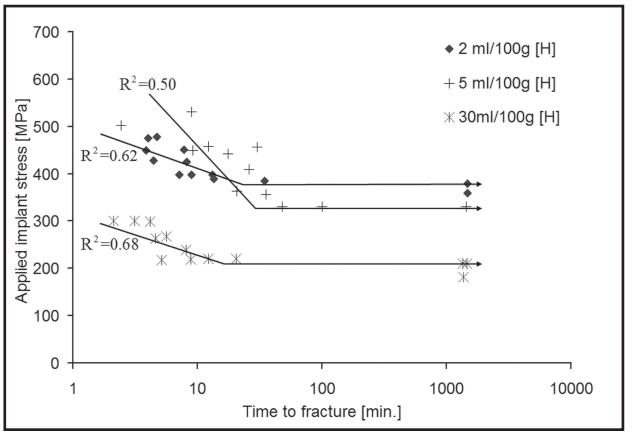

Fig. 4 — Effect of H on the implant test results for steel E: 0.58 (CE) at $t_{800/500}$ of 4.5 s.

were used to calculate the cooling time from 800° to 500°C ($t_{800/500}$), which is a very critical cooling time at which the austenitic microstructure transformations are characterized (Ref. 24). Adam's heat transfer model for a 3-D heat flow (i.e., for a thick plate) can be represented as in Equation 2, while Equation 3 can be used to calculate the cooling time for a 2-D heat flow (i.e., for a thin plate) (Refs. 21, 23, 25). The critical thickness, identifying which equation is to be used, can be calculated using Equation 4 (Refs. 21, 23). If the implant test heat sink (i.e., backing plate) is thinner than the critical thickness, it is a 2-D heat flow; on the other hand, if the heat sink is thicker than the critical thickness, it is a 3-D heat flow (Refs. 21, 23).

$$t_{T_1/T_2} = \left[\frac{(EI/v)fm}{2\pi k}\right]\left[\frac{T_1 - T_2}{(T_2 - T_o)(T_1 - T_o)}\right] \quad (2)$$

where $t_{T1/T2}$ is the cooling time (s) from T_1 to T_2 at initial plate temperature T_o (for $t_{800/500}$: T_1 = 800°C, T_1 = 500°C, and T_o = 25°C), E is the arc voltage (V), v is the welding speed (mm/s), I is the arc current (A), f is the arc efficiency (f= 80% for SMAW and GMAW processes (Ref. 23)), m is a constant related to the weld joint (1 for bead on plate, ⅔ for T-joint (Ref. 23)), and k is the thermal conductivity of the metal (k = 0.028 J.mm^{-1}.S^{-1}.C^{-1} for DIN: St 37-2 (Ref. 23)).

$$t_{T_1/T_2} = \left[\frac{1}{4\pi k \rho_S}\right]\left[\frac{(EI/v)fm}{S}\right]^2 \left[\frac{1}{(T_2 - T_0)^2} - \frac{1}{(T_1 - T_0)^2}\right] \quad (3)$$

where ρ_S is the volumetric specific heat of the heat sink (ρ_S = 0.0044 J.mm^{-3}.°C^{-1} for DIN: St 37-2 (Ref.23)), and S is the thickness of the heat sink in mm.

$$Sc = \left(\left[\frac{(EI/v)fm}{2\rho_s}\right]\left[\frac{1}{(T_2 - T_0)} + \frac{1}{(T_1 - T_0)}\right]\right)^{1/2} \quad (4)$$

where Sc is the critical thickness.

Table 5 shows both the calculated and the measured values of $t_{800/500}$ at different applied welding conditions used during the implant tests. The Adam's model results for 2-D heat flow were slightly higher than the measured values of $t_{800/500}$; this can be attributed to diminishment of the effect of the surface heat transfer in the 2-D flow of the Adam's model. However, there is still a close similarity between the measured and the calculated values of $t_{800/500}$. Additionally, by applying the coefficient of determination (R^2), the goodness of fit for the linear relationship between the measured and the calculated values of $t_{800/500}$ for the 3-D (i.e., thick plate) heat flow was 0.97, and it was 0.99 for 2-D (i.e., thin plate) heat flow. Therefore, it can be concluded that Adam's model is highly suited for evaluating the cooling time between 800° and 500°C ($t_{800/500}$) for implant test procedures.

For steels with estimated yield strength between 350 and 600 MPa, HIC in HAZ forms the majority of the cracks developed by hydrogen embrittlement, especially with electrodes having low carbon contents (Refs. 4, 6, 12, 13). Additionally, weldments with undermatched weld metal strength are most likely to have HIC in the HAZ (Refs. 4, 26). The base metals and consumables were selected to ensure that HIC is more likely to occur in the base metal; the HAZ coarsened grain region was the area at which hardness was measured because the

Table 2 — Chemical Composition and Carbon Equivalent for Base Metals

Steel Type	Base Metal Sample	Chemical Composition, %											CE, %
		C	Si	Mn	P	S	Cr	Mo	Ni	V	Cu	Al	
C-Mn	A	0.130	0.241	1.400	0.017	0.012	0.034	0.010	0.015	0.001	0.018	0.038	0.38
	B	0.148	0.266	1.380	0.018	0.012	0.029	0.009	0.130	0.005	0.324	0.049	0.42
	C	0.210	0.450	1.250	0.020	0.020	0.120	0.060	0.050	0.070	0.120	0.018	0.48
HSLA	D	0.220	0.210	1.260	0.020	0.012	—	—	0.700	0.130	0.150	0.008	0.52
	E	0.118	0.505	0.528	0.011	0.003	1.320	0.536	0.047	0.010	0.020	0.021	0.58
	F	0.198	0.188	1.060	0.017	0.016	1.250	0.215	0.115	0.010	0.185	0.020	0.69
Implant backing plate (heat sink)		0.063	0.181	0.517	0.028	0.012	0.016	0.014	0.018	0.001	0.017	—	—

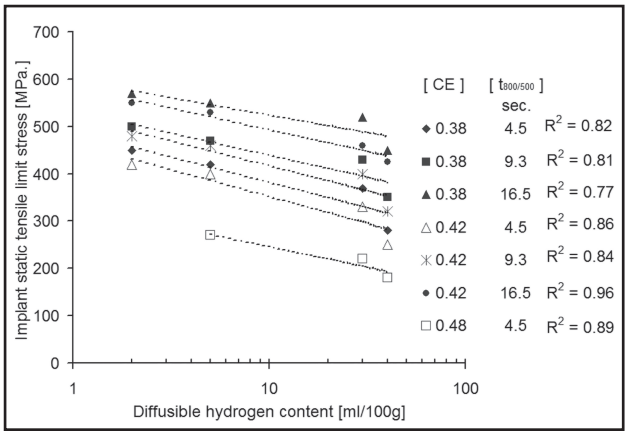

Fig. 5 — Effect of H on σ_{imp} for C-Mn steels at different values of CE and $t_{800/500}$.

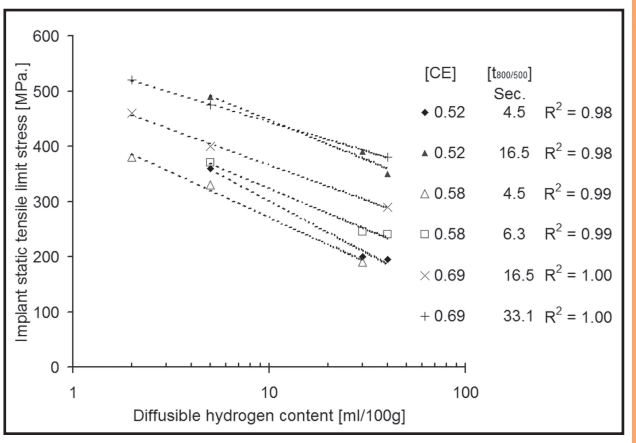

Fig. 6 — Effect of H on σ_{imp} for HSLA steels at different values of CE and $t_{800/500}$.

susceptible HAZ microstructure is expected to be developed in this region (Ref. 27). Figure 2A shows a section through a nonfractured implant pin, while Fig. 2B depicts how the fracture occurred in the implant test specimen within the HAZ coarsened grain region near the weld.

Hardness tests were carried out using a Vickers hardness tester with a 10-kg load (Ref. 19). The hardness was measured in the coarsened grain region of the HAZ on a line tangent to the weld fusion zone. The hardness measurement procedures were applied according to IIW procedures with a 1-mm interval distance between indentations (Refs. 19, 28).

Results Discussion and Modeling

The three major welding factors affecting σ_{imp} and HV_{10MAX} are as follows (Refs. 1–4, 19): 1) the cooling time between 800° and 500°C ($t_{800/500}$); 2) the base metal carbon equivalent (CE); and 3) the diffusible hydrogen content (H). There are some other minor factors that also affect the values of σ_{imp} and HV_{10MAX} (i.e., the susceptibility to HIC), such as the carbon content and the yield strength (Refs. 4, 6, 12, 13, 29); however, the present study focuses on the three major effective factors (i.e., $t_{800/500}$, CE, and H) and their effect on σ_{imp} and HV_{10MAX}. In this study, these three major effective factors were considered the essential variables that were used to develop the mathematical models for both σ_{imp} and HV_{10MAX}.

The following part is divided into two main sections: the first section, assessment of HIC susceptibility, is to demonstrate the observed effects of $t_{800/500}$, CE, and H on σ_{imp} and HV_{10MAX}; the second section, modeling of HIC susceptibility, is to illustrate how these three welding factors (i.e., $t_{800/500}$, CE, and H) are interactively integrated to affect σ_{imp} and HV_{10MAX}; additionally, the second section discusses how to incorporate the interactively integrated effect of the three major welding factors into simplified mathematical models developed to simulate σ_{imp} and HV_{10MAX}.

Table 3 — Electrodes Designations, Chemical Composition, and the Mechanical Properties of Deposited Weld Metal for Welding Electrodes

Type of Flux	Electrode Type Classifications (AWS Designation)	Electrode Diameter (mm)	Chemical Composition, % C	Si	Mn	Mo	Mechanical Properties Yield Point MPa.	Tensile Strength MPa.
Cellulose	A5.05-81 E7010-G	3.25 4.00 5.00	0.14	0.14	0.60	0.20	420	480–590
Rutile	A5.01-81 E6013	3.25 4.00 5.00	0.06	0.40	0.50	—	390	470–590
Basic	A5.01-81 E7018	3.25 4.00 5.00	0.05	0.06	0.90	—	400	510–630
Solid wire CO_2-shielding gas	A5.18-79 ER7S-6	1.0 1.2	0.08	0.90	1.5	—	460	560

Assessment of HIC Susceptibility

Figures 3 and 4 show implant stress-time curves that indicate the effect of different values of the diffusible hydrogen content (H) on the implant test results for both C-Mn steel with CE of 0.42 and HSLA steel with CE of 0.58, respectively, at $t_{800/500}$ of 4.5 s. The first part of these implant stress-time curves was developed as a result of the different stresses that were applied until the implant limit stress (σ_{imp}) was reached, which is represented by the horizontal lines in the curves. The logarithmic regression was used to plot the linear relationship in the first part of the implant stress-time curves. These developed linear relationships were plotted not to represent any physical property except the general trend of the first part of the implant stress-time curves (i.e., to demonstrate that the time to fracture increased by decreasing the applied static stress). R^2 values in Figs. 3 and 4 represent the goodness of fit of the logarithmic regression used to plot the first part of the curves. The horizontal lines in Figs. 3 and 4 demonstrate that the value of σ_{imp} decreases by increasing H, and this increases the risk of HIC at a constant value of $t_{800/500}$. Using the logarithmic regression, Figs. 5 and 6 show the relationship between σ_{imp} and H for both C-Mn and HSLA steels, respectively, at different values of CE and $t_{800/500}$. Generally, Figs. 5 and 6 illustrate that at certain $t_{800/500}$ and CE when the value of H decreases, the value of σ_{imp} increases, and this reduces the susceptibility to HIC.

The implant test results for both C-Mn steel with CE of 0.42 and HSLA steel with CE of 0.58 were plotted at H of 30 mL/100

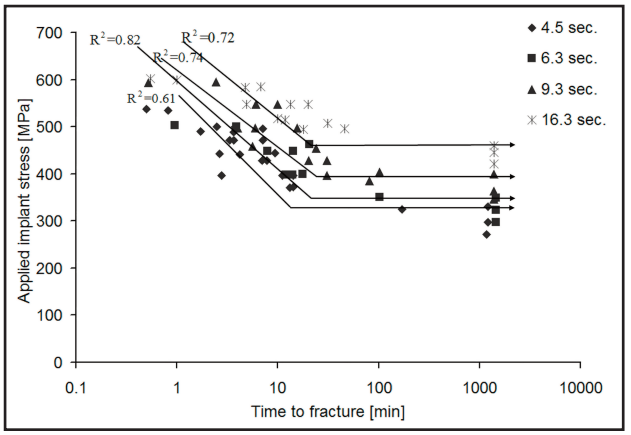

Fig. 7 — Effect of $t_{800/500}$ on the implant test results for steel B: 0.42 (CE) at H of 30 mL/100 g.

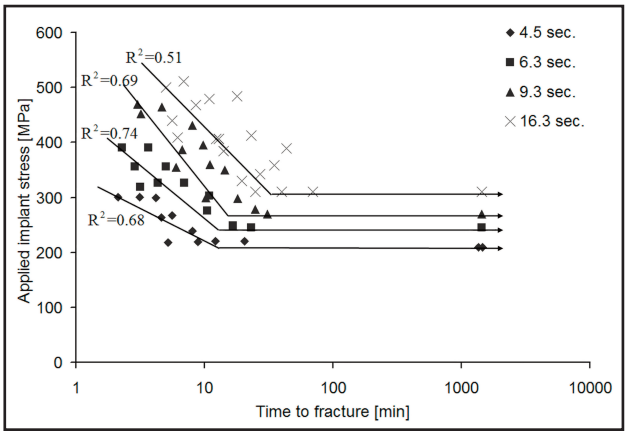

Fig. 8 — Effect of $t_{800/500}$ on the implant test results for steel E: 0.58 (CE) at H of 30 mL/100 g.

g and different values of $t_{800/500}$, as shown in Figs. 7 and 8, respectively. As depicted in Figs. 7 and 8, when the cooling time between 800° and 500°C ($t_{800/500}$) increased, the implant static tensile limit stress (σ_{imp}) increased, lessening the susceptibility to HIC. The same result can be concluded from Figs. 9 and 10, which show the σ_{imp}-$t_{800/500}$ relationship conducted by the logarithmic regression for both C-Mn and HSLA steels, respectively, at different values of CE and H. Figure 11A–C shows how $t_{800/500}$ affects the development of the susceptible HAZ microstructure. Figure 11A shows a ferrite pearlite hot-rolled microstructure of the base metal A: 0.38% CE (Ref. 19). This microstructure was transformed into a Widmanstätten ferrite microstructure in the HAZ of the implant test specimen at $t_{800/500}$ value of 4.5 s (Ref. 19), as shown in Fig. 11B. In Fig. 11C, as $t_{800/500}$ increased to 16.5 s, the ferrite pearlite base metal structure was transformed into a refined acicular ferrite with a cleavage shape structure (Ref. 19). This change in the HAZ microstructure from the Widmanstätten ferrite to the acicular ferrite reduced HV_{10MAX} from 385 to 330, and increased the implant static tensile limit stress (σ_{imp}) from 450 to 565 MPa, respectively, at H of 2 mL/100 g (Ref. 19).

Figures 12 and 13 indicate the effect of carbon equivalent (CE) on the results of the implant test at $t_{800/500}$ of 9.3 s for C-Mn steels and at $t_{800/500}$ of 6.3 s for HSLA steels, respectively, at H of 40 mL/100 g. Decreasing CE values caused an increase in the measured values of the implant static tensile limit stress (σ_{imp}), as shown by the horizontal lines in Figs. 12 and 13. The same behavior is confirmed through Figs. 14 and 15, as the linear regression was used to show the relationship between σ_{imp} and carbon equivalent (CE) for both C-Mn and HSLA steels, respectively, at different values of $t_{800/500}$ and H. Therefore, as concluded from Figs. 12–15, σ_{imp} decreases by increasing CE, which promotes the susceptibility to HIC.

Using the logarithmic regression, Figs. 16 and 17 represent the relationship between HV_{10MAX} and $t_{800/500}$ for C-Mn and HSLA steels, respectively, at different values of CE. The maximum HAZ hardness (HV_{10MAX}) was increased by decreasing the cooling time between 800° and 500°C ($t_{800/500}$). On the other hand, decreasing CE caused HV_{10MAX} to decrease at a certain $t_{800/500}$, as depicted in Figs. 18 and 19, using the linear regression, for C-Mn and HSLA steels, respectively.

Modeling of HIC Susceptibility

Cooling time between 800° and 500°C ($t_{800/500}$) and carbon equivalent (CE) influence the microstructure ability to produce a certain maximum HAZ hardness (HV_{10MAX}), which consequently can be used to assess the developed microstructure in HAZ (Refs. 4, 12–16). Therefore, HV_{10MAX} can be assumed to be the reason by which $t_{800/500}$ and CE affect σ_{imp}. Hence, it can be concluded that the main welding factors affecting σ_{imp} are the maximum HAZ hardness (HV_{10MAX}), and the diffusible hydrogen content (H). On the other hand, the welding factors affecting HV_{10MAX} are the cooling time between 800° and 500°C ($t_{800/500}$), and the carbon equivalent (CE).

To develop the models that predict the values of σ_{imp} and HV_{10MAX}, the effect of each welding factor on σ_{imp} and HV_{10MAX}

Table 4 — Diffusible Hydrogen Content for Deposited Weld Metal

Process	Coating	Consumable Electrode Type: Electrode Classifications (AWS Designation)	Electrode Conditions	Heat Input Used in the Evaluation, kJ/mm	Diffusible Hydrogen Content H (IIW), mL/100 g
SMAW	Cellulose	A5.05-81 E7010-G	Not Recommended	1.7	40
SMAW	Rutile	A5.01-81 E6013	1 h at temperature 150°C	1.7	30
SMAW	Basic	A5.01-81 E7018	2 h at temperature 260°C	1.7	5
GMAW	Solid Wire CO_2 Shielding Gases	A5.18-79 ER70S-6	Not Recommended	1.7	2

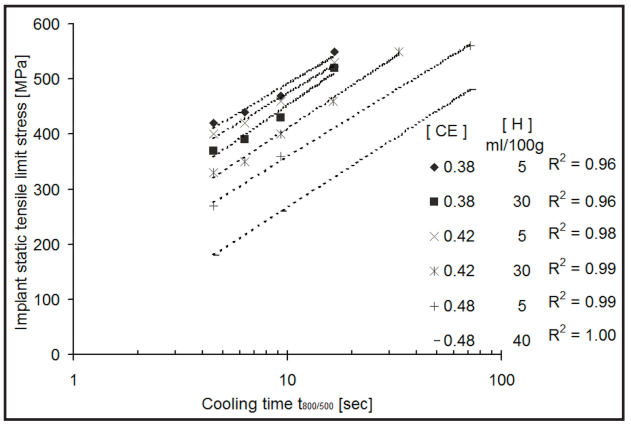

Fig. 9 — Effect of $t_{800/500}$ on σ_{imp} for C-Mn steel at different values of CE and H.

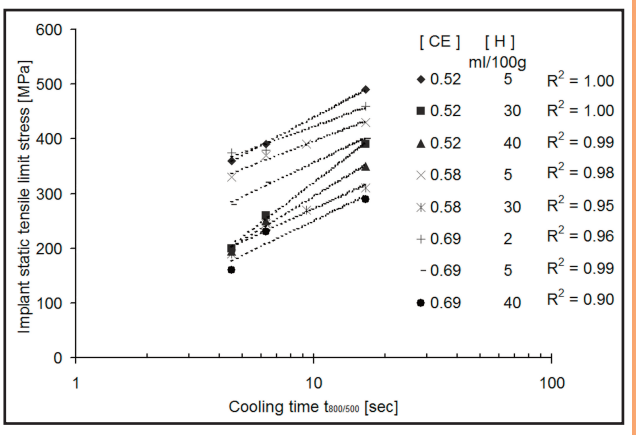

Fig. 10 — Effect of $t_{800/500}$ on σ_{imp} for HSLA steel at different values of CE and H.

have to be evaluated. Pearson's product-moment coefficient (P_{pm}) can provide an indication of the dependency or independency of two numerical values with regard to each other (Refs. 30–32). Therefore, Pearson's product-moment coefficient (P_{pm}) can be used as a tool to identify the dominating welding factor affecting either σ_{imp} or HV_{10MAX} by evaluating the dependency of σ_{imp} and HV_{10MAX} on each welding factor that affects each one of them. Equation 5 represents the statistical function used to calculate P_{pm} (Ref. 33).

$$P_{pm}(x,y) = \frac{\sum_{i=1}^{n}(x_i-\bar{x})(y_i-\bar{y})}{\sqrt{\sum_{i=1}^{n}(x_i-\bar{x})^2\sum_{i=1}^{n}(y_i-\bar{y})^2}} \quad (5)$$

where P_{pm} (x,y) is Pearson's product-moment coefficient for two numerical parameters (i.e., x and y), n is the number of readings for parameters x and y, $\bar{x}$ is the average of parameter x readings, $\bar{y}$ is the average of parameter y readings, and i is the counter of the readings number n.

P_{pm} can take values from 1.00 to –1.00. At P_{pm} = 1.00, there is a perfect direct correlation between the two numerical parameters. At P_{pm} = 0.00, there is no correlation at all between the numerical parameters. For P_{pm} = –1.00, there is a perfect inverse correlation between the two numerical parameters.

As illustrated previously, the main welding factors controlling σ_{imp} can be considered to be the maximum HAZ hardness (HV_{10MAX}) and the diffusible hydrogen content (H). Table 6 shows the values of P_{pm} between σ_{imp} and its controlling welding factors (i.e., HV_{10MAX} and H) for the tested C-Mn steels and HSLA steels. For C-Mn steels (i.e., CE: 0.38 to CE: 0.48), the values of P_{pm} for the σ_{imp}-HV_{10MAX} relationship are relatively high, which means that HV_{10MAX} is the dominating welding factor affecting σ_{imp}, and the negative sign is a result of the inverse correlation between HV_{10MAX} and σ_{imp}. However, the dominating effect of HV_{10MAX} over σ_{imp} was reduced for HSLA steels (i.e., CE: 0.52 to 0.69), and H became the dominating welding factor that affected σ_{imp}; therefore, it can be concluded that the HIC susceptibility for the HSLA steel category is mainly dominated by the diffusible hydrogen content (H). This could be attributed to the relatively heavy existence of some alloying elements in the composition of HSLA steels. These alloying elements increase the effect of the diffusible hydrogen content (H) on the susceptibility to HIC. To illustrate, the vanadium (V) percentage in steel D (CE: 0.52) was relatively high (V: 0.13%) compared to the vanadium percentage in other steels. The increase in the vanadium percentage promoted the amount of the absorbed hydrogen for a given value of the diffusible hydrogen content (H) (Ref. 34); therefore, the effect of the diffusible hydro-

Table 5 — Implant Test Welding Conditions and Cooling Times from the Thermocouple and from the Adam's Model

Welding Conditions		Electrode Type: Cellulose (E7010-G) – Rutile (E6013) – Basic (E7018)			Solid Wire CO_2 Shielding Gases ER70S-6		
Electrode Diameter (mm)		3.25	4.0	5.0	1.0	1.2	1.2
Current (A)		125	170	225	200	250	250
Voltage (V)		24	25	28	27	30	30
Welding Speed (mm/s)		2.5	2.5	2.5	4.5	4.5	3
Heat Input (kJ/mm)		1.2	1.7	2.5	1.2	1.7	2.5
$T_{800/500}$ (s)	Thick, 30 mm, using the thermocouple	4.7	5.8	10.1	4.9	6.5	9.8
	Thick, 30 mm, using Adam's model	4.5	6.3	9.3	4.5	6.3	9.3
	Thin, 10 mm, using the thermocouple	15.7	29.7	67.3	14.8	30.9	65.1
	Thin, 10 mm, using Adam's model	16.5	33.1	71.5	16.5	33.1	71.5

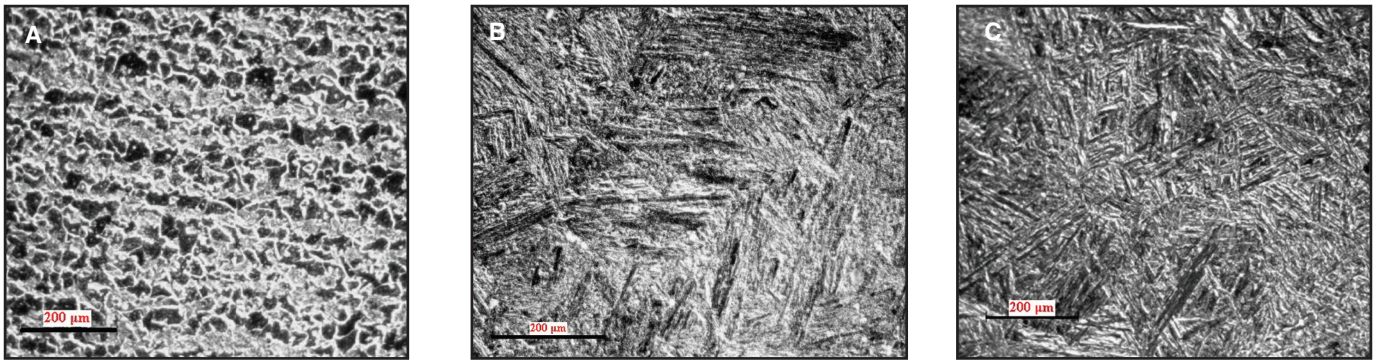

Fig. 11 — Microstructure images of (Ref.19): A — The C-Mn steel A: 0.38 CE base metal; B — a Widmanstätten ferrite in the coarsened grain HAZ region at $t_{800/500}$ of 4.5 s; and C — an acicular ferrite in the HAZ coarsened grain region at $t_{800/500}$ of 16.5 s.

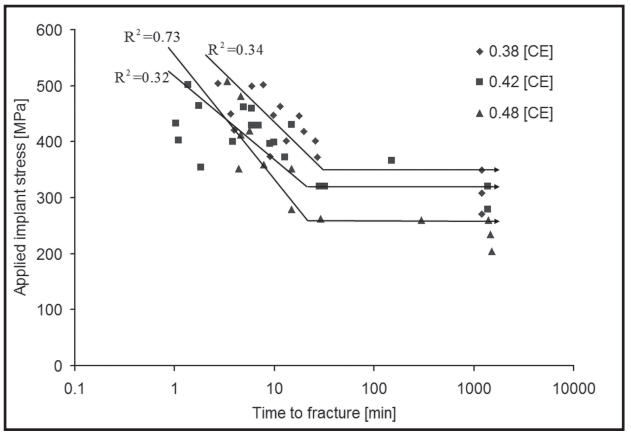

Fig. 12 — Effect of base metal CE on the results of the implant test for A: 0.38 (CE), B: 0.42 (CE), and C: 0.48 (CE) at H of 40 mL/100 g and $t_{800/500}$ of 9.3 s.

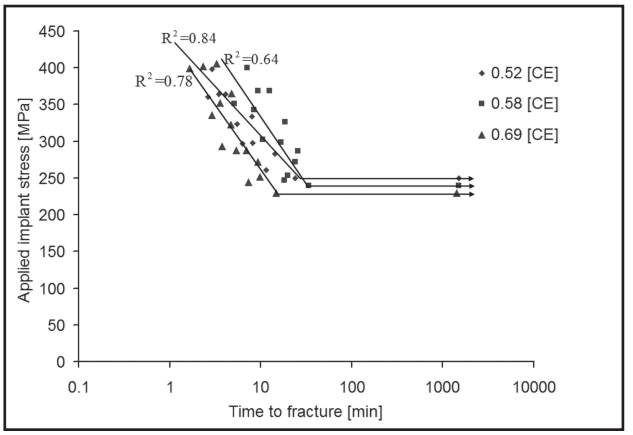

Fig. 13 — Effect of base metal CE on the results of the implant test for steels D: 0.52 (CE), E: 0.58 (CE), and F: 0.69 (CE) at H of 40 mL/100 g and $t_{800/500}$ of 6.3 s.

gen content (H) on the susceptibility to HIC was increased; additionally, the percentage of other alloying elements such as nickel (Ni) in the same D (CE: 0.52) steel was relatively a high percentage (Ni: 0.7%), and this increased the amount of the absorbed hydrogen (Refs. 35, 36). For other HSLA steels, the relatively high percentage of chromium (Cr) and molybdenum (Mo) in both steel E (CE: 0.58) and steel F (CE: 0.69) acted interactively to increase the susceptibility to HIC as a result of increasing the diffused hydrogen (Ref. 20). However, from Table 6, as the CE range was increased to include both C-Mn steels and HSLA steels (i.e., for the overall CE range from 0.38 to 0.69), HV_{10MAX} can be considered as the overall dominating welding factor that affects σ_{imp} in steel weldments. The overall values of P_{pm} for HV_{10MAX} are relatively high (P_{pm} = –0.71); therefore, a linear mechanistic model can be proposed to simulate the relationship between σ_{imp} and HV_{10MAX} as follows:

$$\sigma_{imp} = \alpha + \beta\, HV_{10MAX} \qquad (6)$$

where α and β are parameters assumed to be functions of the diffusible hydrogen content (H).

Figures 5 and 6 show the relationship between σ_{imp} and H could be represented using a logarithmic model. Therefore, the parameters α and β in Equation 6 could be represented as a function of H using the logarithmic model shown in Equations 7 and 8, respectively.

$$\alpha = \alpha_a + \alpha_b \ln(H) \qquad (7)$$

where α_a and α_b are base metal parameters.

$$\beta = \beta_a + \beta_b \ln(H) \qquad (8)$$

where β_a and β_b are base metal parameters.

From Equations 6–8, the developed model of σ_{imp} can be represented as follows:

$$\sigma_{imp} = \alpha_a + \beta_a HV_{10MAX} + \ln(H)(\alpha_b + \beta_b HV_{10MAX}) \qquad (9)$$

where σ_{imp} is the implant static tensile limit stress, HV_{10MAX} is the maximum HAZ hardness, H is the diffusible hydrogen content, α_a and α_b are the base metal parameters in Equation 7, and β_a and β_b are the base metal parameters in Equation 8.

Using Levenberg-Marquardt, a modified version of the Gauss-Newton method (Ref. 37), the optimized solutions for the developed model parameters in Equation 9 were calculated. Table 7 shows the optimized solutions of the parameters α_a, α_b, β_a, and β_b in Equation 9 for the categories of tested steels.

Using the parameter values in Table 7, Figs. 20–22 were plotted showing that the values of σ_{imp} calculated by the developed model (σ_{impC}), in Equation 9, closely match

Table 6 — Pearson's Product-Moment Coefficients between σ_{imp} and Its Controlling Welding Factors

Steel	P_{pm} for σ_{imp}-HV_{10MAX}	P_{pm} for σ_{imp}-H
C-Mn (CE: 0.38 to CE: 0.48)	–0.77	–0.65
HSLA (CE: 0.52 to CE: 0.69)	–0.47	–0.76
C-Mn and HSLA (CE: 0.38 to CE: 0.69)	–0.71	–0.64

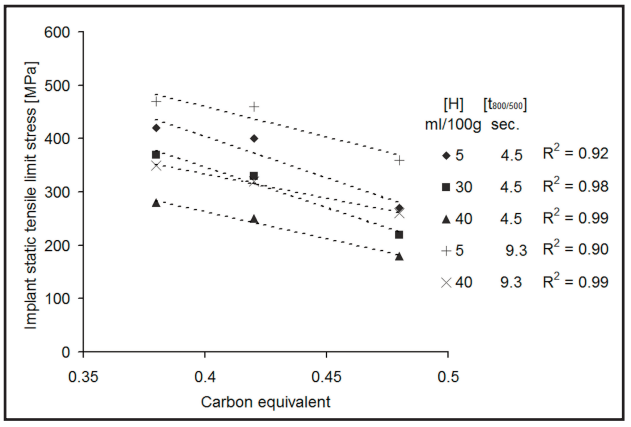

Fig. 14 — Effect of CE on σ_{imp} for C-Mn steels at different values of H and $t_{800/500}$.

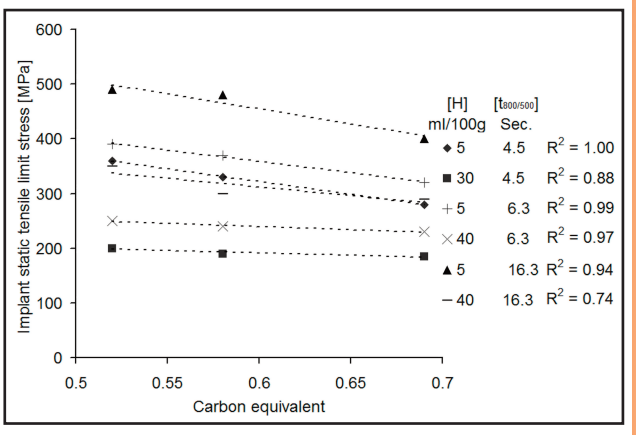

Fig. 15 — Effect of CE on σ_{imp} for HSLA steels at different values of H and $t_{800/500}$.

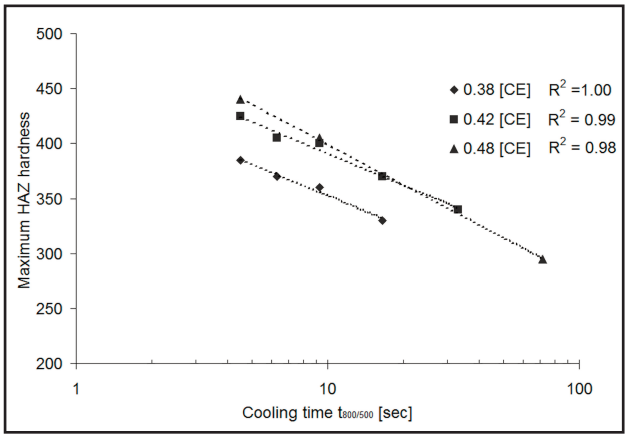

Fig. 16 — Effect of $t_{800/500}$ on maximum HAZ hardness (HV_{10MAX}) for C-Mn steels.

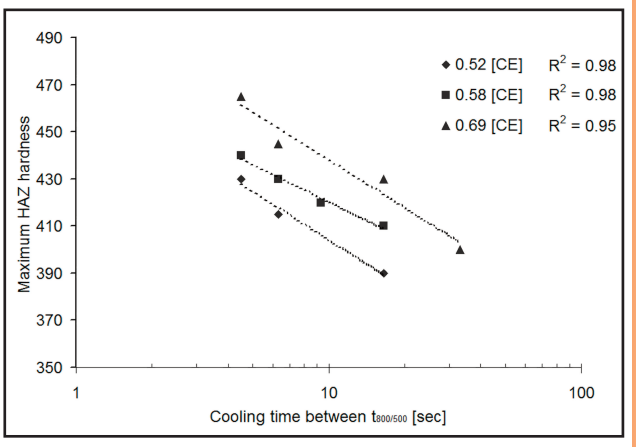

Fig. 17 — Effect of $t_{800/500}$ on HV_{10MAX} for HSLA steels.

the values of σ_{imp} measured from the implant tests (σ_{impM}) for CE ranges of 0.38–0.48 (i.e., C-Mn steels), 0.52–0.69 (i.e., HSLA steels), and 0.38–0.69 (i.e., both C-Mn and HSLA steels), respectively.

The second parameter that can be used to assess HAZ susceptibility to HIC is the maximum HAZ hardness (HV_{10MAX}), which is affected by $t_{800/500}$ and CE (Refs. 1–4, 19). Table 8 shows the values of P_{pm} for HV_{10MAX}-$t_{800/500}$ and HV_{10MAX}-H relationships. For both the C-Mn steels category (with CE ranging between 0.38 and 0.48) and HSLA steels category (with CE ranging between 0.52 and 0.69), the dominating welding factor affecting HV_{10MAX} is $t_{800/500}$, as shown in Table 8. By increasing the CE domain to cover the range between 0.38 and 0.69, the P_{pm} for the HV_{10MAX}-$t_{800/500}$ relationship was lowered to –0.45. This can be attributed to the lack of linearity in the HV_{10MAX}-$t_{800/500}$ relationship, as shown in Figs. 16 and 17. On the other hand, the P_{pm} for HV_{10MAX}-CE increased to –0.70, which can be attributed to the linearity in the relationship between HV_{10MAX} and CE, as shown in Figs. 18 and 19. Therefore, $t_{800/500}$ can still be assumed to be the dominating welding factor affecting HV_{10MAX} for both C-Mn and HSLA steels. For C-Mn and HSLA steels, the relationship between $t_{800/500}$ and HV_{10MAX} is a logarithmic relationship, as shown in Figs. 16 and 17, respectively; therefore, the relationship between $t_{800/500}$ and HV_{10MAX} can be represented using a logarithmic mechanistic model as follows:

$$HV_{10MAX} = \xi + \psi \ln(t_{800/500}) \quad (10)$$

Table 7 — The Optimized Values for Parameters α_a, α_b, β_a, and β_b in Equation 9

Parameter	Value for C-Mn	Value for HSLA	Value for C-Mn and HSLA
α_a	1060.38	1509.98	1011.04
α_b	42.72	44.81	102.87
β_a	–1.42	–2.40	–1.26
β_b	–0.23	–0.26	–0.39

where ξ and ψ are parameters that can be considered as functions of carbon equivalent (CE).

Figures 18 and 19 show a linear relationship between CE and HV_{10MAX}; therefore, ξ and ψ, assumed to be a function of CE in Equation 10, can be represented in linear relationships with CE as in Equations 11 and 12, respectively.

$$\xi = \xi_a + \xi_b CE \quad (11)$$

where ξ_a and ξ_b are base metal parameters.

$$\psi = \psi_a + \psi_b CE \quad (12)$$

where ψ_a and ψ_b are base metal parameters.

From Equations 10–12, the developed model for HV_{10MAX} in Equation 10 can be rewritten as follows:

$$HV_{10MAX} = \xi_a + \psi_a \ln(t_{800/500}) + CE(\xi_b + \psi_b \ln(t_{800/500})) \quad (13)$$

where HV_{10MAX} is the maximum HAZ hardness, $t_{800/500}$ is the cooling time between 800° and 500°C, ξ_a and ξ_b are the base metal parameters in Equation 11,

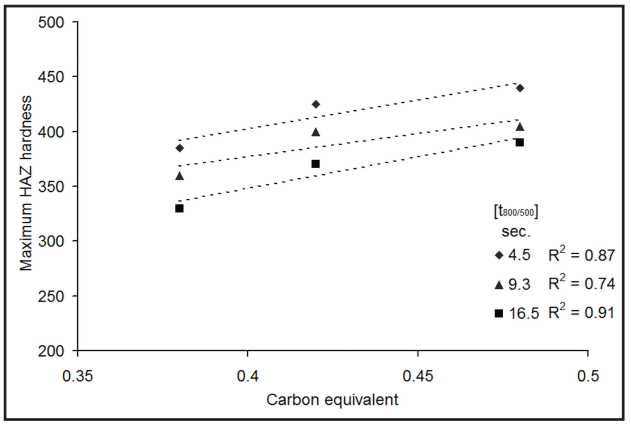

Fig. 18 — Effect of CE on HV_{10MAX} for C-Mn steels.

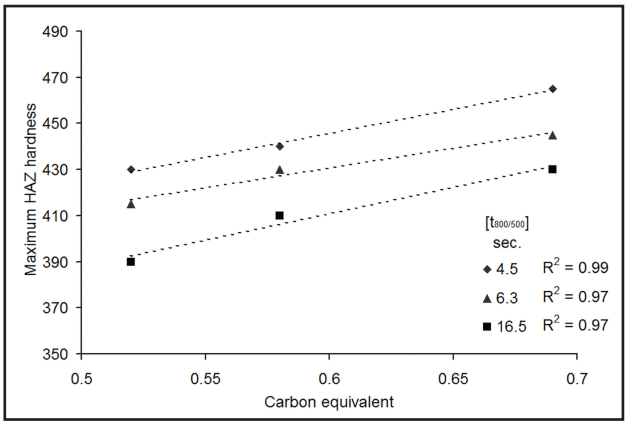

Fig. 19 — Effect of CE on HV_{10MAX} for HSLA steels.

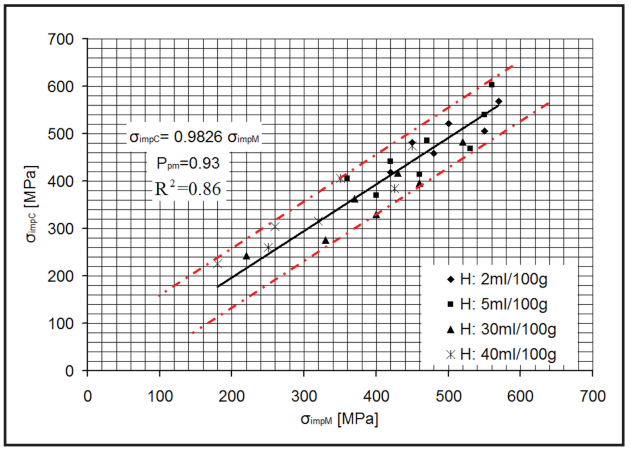

Fig. 20 — The relation between the measured σ_{imp} (σ_{impM}) and the calculated σ_{imp} (σ_{impC}) for C-Mn steels.

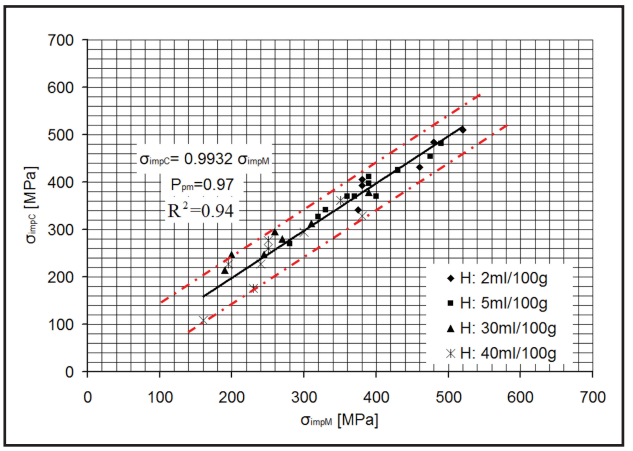

Fig. 21 — The relation between the measured σ_{imp} (σ_{impM}) and the calculated σ_{imp} (σ_{impC}) for HSLA steels.

and ψ_a and ψ_b are the base metal parameters in Equation 12.

Using the Levenberg-Marquardt method, the optimized solutions for parameters ξ_a, ξ_b, ψ_a, and ψ_b in Equation 13 are shown in Table 9 for the tested categories of steels.

Figures 23–25 demonstrate a good match between the measured HV_{10MAX} and the values of HV_{10MAX} calculated using the model developed in Equation 13 for the CE ranges of 0.38–0.48, 0.52–0.69, and 0.38–0.69, respectively.

Conclusion

The effect of each welding factor (i.e., diffusible hydrogen content (H), cooling time between 800° and 500°C ($t_{800/500}$) and carbon equivalent (CE)) on HIC susceptibility was investigated. The susceptibility of HAZ to HIC was assessed using implant static tensile limit stress (σ_{imp}) and maximum HAZ hardness (HV_{10MAX}). The experimental results showed that σ_{imp} increased, decreasing the susceptibility to HIC, by increasing $t_{800/500}$; on the other hand, σ_{imp} decreased, increasing the susceptibility to HIC, by increasing CE and H. Additionally, it was shown through experimental results that HV_{10MAX} increases by increasing CE or reducing $t_{800/500}$, and this increases the susceptibility to HIC.

Based on the calculated values of P_{pm}, the dominating factor affecting σ_{imp} for the C-Mn steel category (i.e., for CE: 0.38–0.48) was found to be HV_{10MAX}, while the dominating factor affecting σ_{imp} was H for the HSLA steels category (i.e., for CE: 0.38–0.48); this can be attributed to relatively high percentages of the alloying elements that exist in HSLA steels, such as V, Ni, Cr, and Mo. The dominating welding factor affecting HV_{10MAX} was found to be $t_{800/500}$ for both C-Mn steels and HSLA steels.

Mechanistic models, linear and logarithmic, were used to develop simplified models that successfully simulated both σ_{imp} and HV_{10MAX}. The σ_{imp} model was developed as a function of HV_{10MAX} and diffusible hydrogen content (H), while the HV_{10MAX} model was developed as a function of the cooling time between 800° and 500°C ($t_{800/500}$) and the base metal carbon equivalent (CE). For C-Mn (CE: 0.38–0.48) or HSLA (CE: 0.52–0.69), the results from the developed models have a good match with the experimental results for both σ_{imp} and HV_{10MAX}; furthermore,

Table 8 — Pearson's Product-Moment Coefficients between HV_{10MAX} and Its Controlling Welding Factors

Steel	P_{pm} for HV_{10MAX}-$t_{800/500}$	P_{pm} for HV_{10MAX}-CE
C-Mn (CE: 0.38 to CE: 0.48)	–0.68	0.44
HSLA (CE: 0.52 to CE:0.69)	–0.68	0.44
C-Mn and HSLA (CE: 0.38 to CE: 0.69)	–0.45	0.70

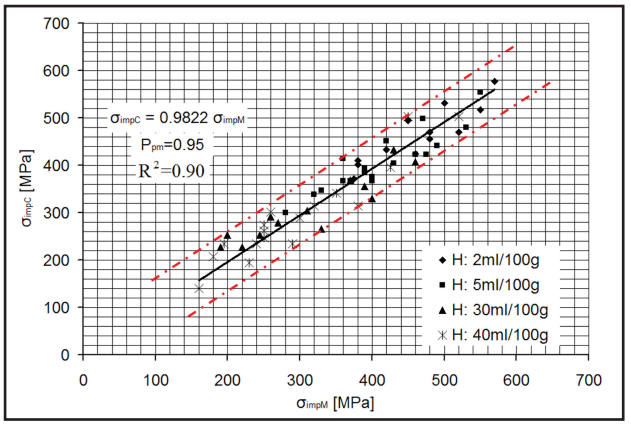

Fig. 22 — The relation between the measured σ_{imp} (σ_{impM}) and the calculated σ_{imp} (σ_{impC}) for C-Mn and HSLA steels.

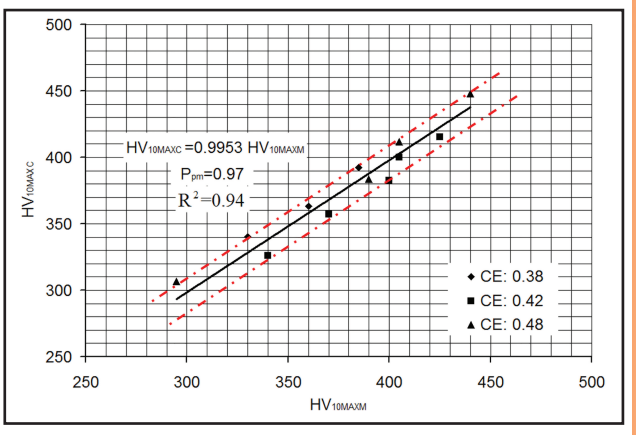

Fig. 23 — The relation between the measured HV_{10MAX} (HV_{10MAXM}) and the calculated HV_{10MAX} (HV_{10MAXC}) for C-Mn steels.

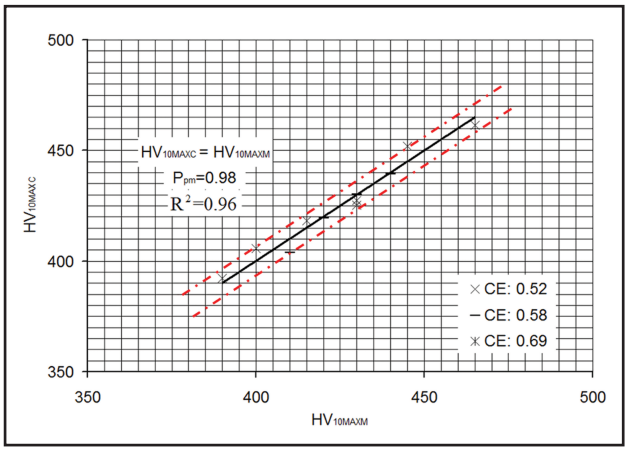

Fig. 24 — The relation between the measured HV_{10MAX} (HV_{10MAXM}) and the calculated HV_{10MAX} (HV_{10MAXC}) for HSLA steels.

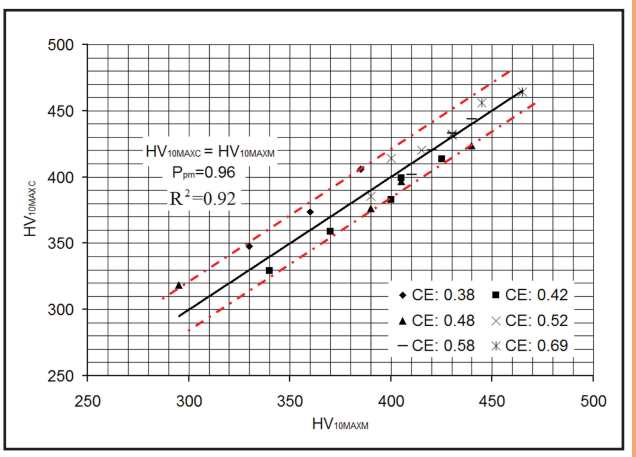

Fig. 25 — The relation between the measured HV_{10MAX} (HV_{10MAXM}) and the calculated HV_{10MAX} (HV_{10MAXC}) for C-Mn and HSLA steels.

the same developed models successfully simulated σ_{imp} and HV_{10MAX} for the whole range of CE, including the two steel categories together (i.e., with CE range between 0.38 and 0.69). The developed models provide the designer with a reliable simplified engineering tool by which the designer can evaluate the maximum HAZ hardness (HV_{10MAX}) and the implant static tensile limit stress (σ_{imp}) in steel weldments.

References

1. Uncic, R. R. 2000. The effect of arc welding parameters on diffusible hydrogen content in steel weldments, in *Welding Engineering 600 Literature Review*. Dept. of Material Science & Engineering, The Ohio State University. Report. Columbus, Ohio.

2. Coe, F. R., and Bailey, N. 1973. *Welding Steels without Hydrogen Cracking*. 2nd ed. p. 150. Abington, Cambridge: Abington Publishing.

3. Kou, S. 2003. *Welding Metallurgy.* 2nd ed. p. 461. Hoboken, N. J.: Wiley-Interscience.

4. Nevasmaa, P. 2003. Predictive model for the prevention of weld metal hydrogen cracking in high-strength multipass welds. PhD thesis. Oulu, Acta, Finland.

5. Savage, W. F., Nippes, E. F., and Homma, H. 1976. Hydrogen induced cracking in HY-80 steel weldments. *Welding Journal* 55(11): 368-s to 376-s.

6. Henry, O. H., and Linnert, G. E. 1965. *Welding Metallurgy; Carbon and Alloy Steels*. 3d ed. Welding technology series, New York, N.Y.: American Welding Society.

7. Coe, F. R., and Chano, Z. 1975. Hydrogen distribution and removal for a single bead weld during cooling. *Welding Research International* 5(1): 33–90.

8. Schwarz, W., Zitter, H., and Wirm, H. 1971. Determination of diffusible hydrogen in the weld deposit from coated wire electrodes. *Schweissen und Schneiden/Welding and Cutting* 23(4): 133–137.

9. Khalil, M. 2000. Evaluation and prediction of heat affected zone cracks in high strength steel weldments. Design and Manufacturing Engineering. PhD thesis, Cairo, Egypt: Cairo University.

10. Gedeon, S. A., and Eagar, T. W. 1990. Assessing hydrogen-assisted cracking fracture modes in high-strength steel weldments. *Welding Journal* 69(6): 213.

11. El-Hebeary, M. R. 1981. Prediction of safe welding condition to avoid cold cracking of welds, in *International Symposium on Ship Technology*. Wilhelm-Pieck-Universitat Rostock.

12. Karppi, R. A. J., Ruusila, J., Toyoda, M., Satoh, K., and Vartiainen, K. 1984. Predicting safe welding conditions with hydrogen cracking parameters. *Scandinavian Journal of Metallurgy* 13(2): 66–74.

13. Karppi, R. A. J. 1982. *Stress Field Parameter for Weld Hydrogen Cracking*. Espoo, Technical Centre of Finland.

14. Hart, P. H. M., and Harrison, P. L. 1987. Compositional parameters for HAZ cracking

Table 9 — The Optimized Values for Parameters ξ_a, ξ_b, Ψ_a, and Ψ_b in Equation 13

Parameter	Value for C-Mn	Value for HSLA	Value for C-Mn and HSLA
ξ_a	170.16	359.74	437.33
ξ_b	743.30	207.93	94.26
ψ_a	3.33	–24.23	–68.54
ψ_b	–114.42	–5.20	62.74

and hardening in C-Mn steels. *Welding Journal* 66(10): 310-s to 322-s.

15. Hart, P. H. M., Matharu, I. S., and Jones, A. R. 1988. The influence of reduced carbon equivalent on HAZ cracking in structural steels. OMAE 1988 Houston, *Proceedings of the Seventh International Conference on Offshore Mechanics and Arctic Engineering.* Volume V: Pipelines, pp. 111–120. Houston, Tex.: ASME.

16. Okuda, N., et al. 1987. Hydrogen-induced cracking susceptibility in high-strength weld metal. *Welding Journal* 66(5): 141-s to 146-s.

17. TI-809-26. 2000. Welding design procedures and inspection. Engineering and Construction Division, Directorate of Military Programs. Report. Washington, DC.

18. Anon. 1985. Cold cracking test methods using implants. *Welding in the World*, Le Soudage Dans Le Monde 23(1-2): 12–20.

19. Fotouh, A., El-Hebeary, R., and El-Shennawy, M. 2013. Integrated empirical modeling approach assessing susceptibility to hydrogen-induced cracking in single-bead steel weldments. Submitted to Journal of Manufacturing Science and Engineering (ASME).

20. Liou, H. Y., Shieh, R. I., Wei, F. I., and Wang, S. C. 1993. Roles of microalloying elements in hydrogen induced cracking resistant properties of HSLA steel. *Corrosion* 49(5): 389–398.

21. Poorhaydari, K., Patchett, B. M., and Ivey, D. G. 2005. Estimation of cooling rate in the welding of plates with intermediate thickness. *Welding Journal* 84(10): 149-s to 155-s.

22. Easterling, K. E. 1992. *Introduction to the Physical Metallurgy of Welding.* 2nd ed. p. 270. Oxford [England], Boston, Mass.: Butterworth-Heinemann.

23. El-Hebeary, M. R. 1978. Cracking susceptibility of high strength steel welded structuresed. PhD thesis. Budapest, Hungary: Hungarian Academy of Science.

24. Connor, L. P., O'Brien, R. L., and Oates, W. R., editors. 1987. *Welding Handbook.* 8th ed. Miami, Fla.: American Welding Society.

25. Chan, B., Bibby, M. J., and Goldak, J. A. 1992. A software system for computing the HAZ hardness after postweld heat treatment – II. *Canadian Metallurgical Quarterly* 31(3): 203–209.

26. Yatake, T., and Yurioka, N. 1981. Studies of delayed cracking in steel weldments (Report 3). *Journal of the Japan Welding Society* (JWS) 50(3): 291–296.

27. Rollason, E. C. 1973. *Metallurgy for Engineers.* 4th ed. p. 448. London, UK: Edward Arnold.

28. Anon. 1987. Hardness testing in the heat-affected zone of steel welds. *Welding in the World*, Le Soudage Dans Le Monde 25(1-2): 2–11.

29. Yurioka, N., Okumura, M., Kasuya, T., and Cotton, H. J. U. 1987. Prediction of HAZ hardness of transformable steels. *Metal Construction* 19(4): 217r–223r.

30. Stamatis, D. H. 2001. *Six Sigma and Beyond*. Boca Raton, Fla: St. Lucie Press.

31. Pestman, W. R., and Alberink, I. B. 1998. *Mathematical Statistics: Problems and Detailed Solutions*. p. 325. De Gruyter textbook, Berlin; New York, N.Y.: Walter de Gruyter.

32. Lomax, R. G. 2001. *An Introduction to Statistical Concepts for Education and Behavioral Sciences*. p. 520. Mahwah, N.J.: Lawrence Erlbaum Associates.

33. Spiegel, M. R. 1992. *Schaum's Outline of Theory and Problems of Probability and Statistics*. p. 372. Schaum's outline series, New York, N.Y.: McGraw-Hill.

34. Song, X., Pei, P., Zhang, P., and Chen, G. 2006. Effect of vanadium content on hydrogen storage property in Ti-V-Cr alloys. *Rare Metals* 25(6 SUPPL. 1): 374–377.

35. Herms, E., Olive, J. M., and Puiggali, M. 1999. Hydrogen embrittlement of 316L type stainless steel. *Materials Science and Engineering A* 272(2): 279–283.

36. Evans, J. M. 1992. The effect of nickel plating on hydrogen embrittlement of high strength steel. School of Industrial and Manufacturing Science. PhD thesis, London, UK: Cranfield Institute of Technology.

37. Seber, G. A. F., and Wild, C. J. 1989. *Nonlinear Regression.* p. 768. New York, N.Y.: Wiley.

Statement of Ownership, Management and Circulation for U.S. Postal Service (Required by U.S.C. 3685)

1. TITLE OF PUBLICATION: Welding Journal
2. PUBLICATION NO.: ISSN 0043-2296
3. DATE OF FILING: September 26, 2013
4. FREQUENCY OF ISSUE: Monthly
5. NO. OF ISSUES PUBLISHED ANNUALLY: 12
6. ANNUAL SUBSCRIPTION: $120.00
7. MAILING ADDRESS OF KNOWN OFFICE OF PUBLICATION: 8669 NW 36 St., #130, Miami, Florida 33166
8. MAILING ADDRESS OF THE HEADQUARTERS OR GENERAL BUSINESS OFFICES OF THE PUBLISHERS: 8669 NW 36 St., #130, Miami, Florida 33166
9. NAMES AND COMPLETE ADDRESS OF PUBLISHER, EDITOR AND MANAGING EDITOR:
   PUBLISHER: Andrew Cullison, AWS, 8669 NW 36 St., #130, Miami, Florida 33166
   EDITOR: Andrew Cullison, AWS, 8669 NW 36 St., #130, Miami, Florida 33166
   EDITOR: Mary Ruth Johnsen, AWS, 8669 NW 36 St., #130, Miami, Florida 33166
10. OWNER: NAME: American Welding Society,Inc. ADDRESS: AWS, 8669 NW 36 St., #130, Miami,, Florida 33166
11. KNOWN BONDHOLDERS, MORTGAGEES, AND OTHER SECURITY HOLDERS OWNING OR HOLDING 1 PERCENT OR MORE OF TOTAL AMOUNT OF BONDS, MORTGAGES OR OTHER SECURITIES: None
12. The purpose, function, and nonprofit status of this organization and the exempt status for Federal income tax purposes: Has not changed during preceding 12 months
13. Publication Title: Welding Journal
14. Issue date for Circulation Data Below: October 2013
15. EXTENT AND NATURE OF CIRCULATION:

	Average No. Copies Each Issue During Preceding 12 Months	Actual No.Copies of Single Issue Published Nearest to Filing Date
A. Total No. Copies Printed (Net Press Run)	49,702	50,080
B. Paid and/or Requested Circulation		
1. Paid / Requested Outside-County Mail Subscriptions Stated on Form 3541	48,029	48,350
2. Paid In-County Subscriptions Stated on Form 3541	None	None
3. Sales Through Dealers and Carriers, Street Vendor, Counter Sales, and other Non-USPS Paid Distribution	None	None
4. Other Classes Mailed Through the USPS	None	None
C. Total Paid / Requested Circulation	48,029	48,350
D. Free Distribution by Mail (Samples, complimentary and other free)		
1. Outside-County as State on Form 3541	160	164
2. In-County as Stated on Form 3541	None	None
3. Other Classes Mailed Through the USPS	None	None
4. Free Distribution Outside the Mail (Carriers or other means)	None	None
E. Total Free Distribution	160	164
F. Total Distribution	48,189	48,514
G. Copies not Distributed	1,513	1,566
H. Total	49,702	50,080
I. Percent Paid and / or Requested Circulation	99.7%	99.7%

16. Statement of Ownership will be printed in the November 2013 issue of this publication.
I certify that the statements made by above are correct and complete:
Andrew Cullison, Publisher